Alternative Methods for Offshore Wind-Wave Resources and Power Assessments over the Gulf of Thailand and Andaman Sea

Woraluck Hongto[#1], Worachat Wannawong[*2], Donlaporn Saetae[#3], Chaiwat Ekkawatpanit[#4], Peera Sakornmaneerat[#5]

[#]*Department of Civil Engineering, Faculty of Engineering, King Mongkut's University of Technology Thonburi, Bangkok 10140, Thailand*

[1]woraluck.ht@gmail.com, [3]donlaporn.sae@kmutt.ac.th, [4]chaiwat.ekk@kmutt.ac.th and [5]peera2613@gmail.com,

[*]*School of Atmospheric Sciences, Sun Yat-sen University, Guangzhou 510275, China*

[2]worachataj@hotmail.com and wannawong@mail.sysu.edu.cn

Abstract— **Offshore wind and waves are classified as major marine renewable energy sources. A reliable assessment of wind and wave energy resources is important to study over the Gulf of Thailand (GoT) and Andaman Sea (ADS). In this study, the surface wind and wave heights were used to investigate the offshore wind and wave energy resources over the GoT and ADS. Alternative methods for the assessment of wind and wave resources are through analysis of wind speeds, wave periods, fully developed wave height (*Hf*) and significant wave height (*Hs*) using a statistical analysis of 10-year hindcast datasets from QSCAT from NASA associated with WaveWatch-III (WW3) model results from NOAA. A short-term analysis of dynamical simulations and its comparison of the WW3 global model and Simulating WAves Nearshore (SWAN) regional model were also used to investigate the preliminary testing and possibility of offshore wind-wave resources and powers. Results of both models were relatively similar to those of buoys at the offshore locations in a case study of Typhoon Linda 1997 entering the GoT. In this study, the results of WW3 datasets revealed that wind and wave capacities at the lower GoT were in the ranges of 400-800 W m^{-2} and 1-1.5 kWm^{-1}, respectively. Over the ADS, WW3 model datasets with the QSCAT wind data provided wind and wave powers in the ranges of 300-600 W m^{-2} and 2-4 kW m^{-1}, respectively. The WW3 and QSCAT combinations, therefore, could be the potential alternative methods for 10-year long-term assessments of wind and wave power.**

Keywords— **Methods, Wind-Wave, Marine Renewable Energy, Gulf of Thailand, Andaman Sea.**

I. INTRODUCTION

Offshore wind and wave energy is currently one of the marine renewable energy sources with the highest demand. The potential of this energy is considerably larger than other renewable energies. The potential production of wind and wave energy derived from offshore sites is generally higher than that of the onshore wind farms due to the steadier and higher wind speeds presenting in ocean areas. For offshore wind and wave resource assessments, highly accurate wind and wave are paramount. In addition, a realistic assessment of wave energy production heavily relies on an accurate knowledge of the local offshore wind and wave fields since these are the main forcing agents of wind-wave formation and its behavior. The reliable assessments are also necessary to find suitable positions for wind-wave energy converter installation.

Recently, several methods for offshore wind and wave measurements are available. The fully developed wave height (*Hf*) and significant wave height (*Hs*) have been estimated by the simplified method with the WaveWatch-III (WW3) model [1] and Simulating WAves Nearshore (SWAN) model [2]. The wind-wave models can provide offshore wind and wave results with high spatial and temporal resolutions with several scale simulations, ranging from global to coastal scales. However, the ocean wind and wave models probably show deviations due to their inability in accurately representing the local terrain characteristics, e.g., topography and roughness. This may significantly impact the accuracy of wind-wave simulations of the models and respective wind-wave energy productions and assessments.

The present study aimed at investigating the offshore wind-wave resources and power assessments over the GoT and ADS by using the alternative methods. In this study, the highest wind speed and wave height locations obtaining from the *Hf* computed by using the surface wind dataset from the satellite were determined. The *Hs* and wave period derived from the QuikSCAT (QSCAT), National Aeronautics and Space Administration (NASA), and from the WW3 global model data, National Oceanic and Atmospheric Administration (NOAA) were utilized for the alternative methods of offshore wind-wave energy, powers, productions and assessments. Ten years of QSCAT satellite and wind-wave modelled reanalysis/analysis datasets were performed as an integrated assessment of wind-wave power investigations over the GoT and ADS. Additionally, the results of WW3 global model dataset, the SWAN model, and buoys were compared in terms of wind speed, *Hs* and peak wave period using Typhoon Linda 1997 entering the GoT as a case study (no local observations in the ADS). The alternative data analysis and model simulations were utilized for the identification and representation in long-term assessments of offshore wind-wave energy and power. The usage of QSCAT satellite data for a conversion of wind speed to the *Hf* associated with the benefit of WW3 global model data could be applied as the alternative methods of offshore wind-wave resources and power assessments for 10-

year statistical assessments. The combination of QSCAT and WW3 could also be used to consider the possibility of offshore wind-wave resources and powers. These would be novel and progress beyond state of the art in offshore satellite-based wind resource mapping and wind-wave model data analysis. This paper is structured with the research methodology described in section II. Section III contains interpretation of results and discussions. The conclusions are finally presented in section IV.

II. DATA AND METHODOLOGY

A. Study Domain

The study domain covered the GoT and ADS (Fig. 1). Its latitude and longitude ranged from 1°S to 24°N and 90°E to 115°E, respectively. This domain was extended to deep-water swells from the Indian Ocean (IDO) to ADS and the South China Sea (SCS) to GoT under the wave refraction and diffraction with the open sea boundary conditions for the preliminary testing of Typhoon Linda 1997 by using a SWAN model. In this study, the WW3 model was not only used for the Initial and Boundary Conditions (IBCs) of the SWAN model but it was also used for the data analysis for the offshore wind-wave energy resources and power assessments. The H_s, mean wave period and wind speed of WW3 global model datasets were applied for the alternative method of the WW3 model and QSCAT satellite. In the GoT and ADS, superimposition of wind seas with pre-existing swells is found during non-monsoon period, while predominance of swells is observed during monsoon season. Multi-peaked spectrum frequently occurred during January to April in the ADS, while the single-peaked spectrum is mainly found in the southwest and northeast monsoons during June to August in the GoT. Both areas are in the rough sea state (*Hs*>1.5 m) during the monsoon period, and relatively calm (*Hs*<1.5 m) during rest of the year. In this study, the wind speed and its computation for the *Hf* and its power were started by using the QSCAT wind data of outstanding possibility areas of high power density (Table 1). The data analysis of wind speed, *Hs* and mean wave period from the WW3 model datasets were observed. The WRF-SWAN model of fully coupled model [3], [4] will be performed in the future work with wind-wave preliminary results and its comparison between the SWAN-WRF model, WAM-ECMWF Reanalysis Interim (ERAI) and WW3-NCEP Climate Forecast System Reanalysis (CFSR) during Typhoon Linda 1997. The WRF model with 12 km (d01), 4 km (d02) and 1.33 km (d03) horizontal grid resolutions coupled with the SWAN model at 926 m (d01), 463 m (d02) and 46.3 m (d03) high resolutions were initially tested over this domain (Fig. 2). It was run for 72 h starting in November 2-5, 1997 with a time step of 10, 5 and 2 min under the Courant-Friedrichs-Levy (CFL) stability criteria for the ocean and coastal consideration and analysis.

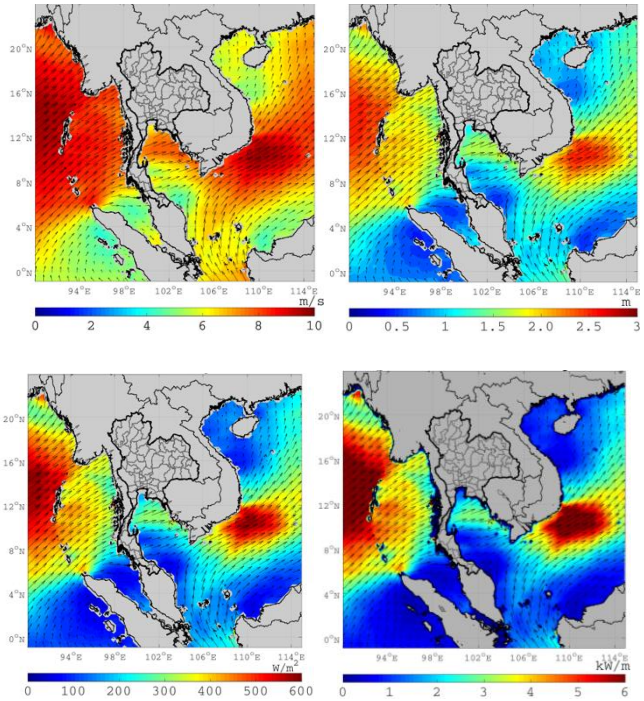

Fig. 1 Overview of wind, *Hf* (top left and right panels) and their power densities (bottom left and right panels) from the QSCAT monthly climatology dataset and its calculation at peak strength in August over the GoT and ADS

TABLE I
AREAS OF OUTSTANDING POSSIBILITY OF HIGH-DENSITY WIND AND WAVE POWER

Index	**Areas of outstanding possibility**			
	Lon. (E)	**Lat. (N)**	**Max. depth(m)**	**Avg. depth(m)**
ADS01	92.0-99.0	4.0-18	3500	1750
ADS02	94.5-99.0	4.0-18	2500	1250
GoT01	99.0-106	5.5-14	90	45.0
GoT02	99.0-104	10-12	70	35.0
GoT03	99.8-104	6.0-9.0	65	32.5

B. QSCAT Data

Quick Scatterometer (QSCAT) observations were collected from October 1999 to October 2009. Multiple radar backscatter measurements over an area obtaining from different viewing angles are organized to wind vector cells. The physical parameter is the equivalent neutral wind at 10 m above the sea surface [5]. Generally, winds cannot be obtained from the QSCAT observations in the coastal zone. SeaWinds scatterometer, the main instrument on the *QSCAT* satellite, is operated at Ku band (13.4 GHz) which is sensitive to rain. Due to rain contamination, winds are biased towards higher wind speeds [6]. In the present study, the QSCAT data from the JPL-NASA with the GMF Ku-2011, which is the gridded wind product at a grid resolution of 25 km by 25 km from Remote Sensing Systems, was utilized for the wind speed and its computation for the *Hf* with power assessments.

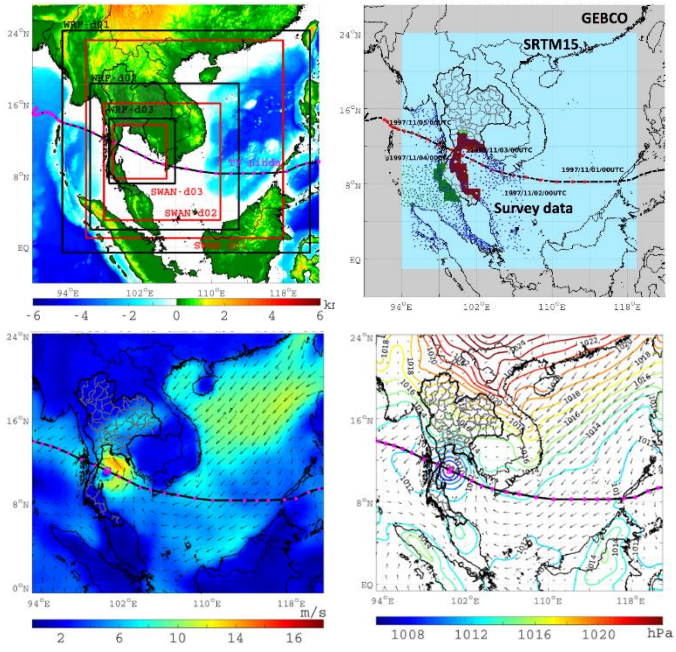

Fig. 2 Bathymetry (top right panel) and computational domains (top left panel) wind and sea level pressure fields (bottom panel) at 18 UTC November of the WRF and SWAN models for a case study of Typhoon Linda 1997.

C. Fully Developed Wave Height and Wave Period

A fully developed sea has the maximum wave size theoretically possible for a wind of a specific strength, duration, and fetch. Further exposure to that specific wind could only cause a dissipation of energy due to the breaking of wave tops and formation of whitecaps. The waves in a specific area have a range of heights. The characteristic height over a period of time is usually expressed as the H_s. However, the H_f would evolve under the action of the wind that represented as

$$H_f = \frac{0.27V^2}{g} \tag{1}$$

The specific term of mean wave period of the possibility of fully developed wave power calculated by

$$\tilde{T} = 9.78\left(\frac{d}{g}\right)^{0.5} \tag{2}$$

where H_f is the fully developed wave height (m), V is the wind velocity (m s^{-1}), $\tilde{T}$ is the specific wave period (s), d is the water depth (m) and g is the gravitational acceleration (9.81 m s^2) [7].

D. WW3 Global Model Datasets and SWAN Model

The WW3 global model datasets produced by NOAA/NCEP was developed under the framework of the WAM model [1]. These datasets have been wildly used in global and regional scale modelling community. They were used to analyze the possibility of offshore wind-wave energy resources and power assessments comparing with the SWAN model package (v.41.20) of fully coupled model [2], [3]. These data and model sets were also utilized for the data analysis of power assessments and compared with the WAM model datasets by the ECMWF reanalysis interim for a short-term comparison. The WW3 model can also implement in different parts of the wave spectral evolution, air-sea interactions and non-linear wave-wave interactions for the global and regional deep water considerations [1]. For the shallow water regions as the GoT, the SWAN model was performed to simulate the offshore wave characteristics [2]. In the region of large scale winds with deep water consideration, the SWAN model was computationally less efficient there with the use of implicit scheme, whereas the WW3 model uses explicit and semi-implicit schemes for source term simulation. The nesting of SWAN in WW3 is, thus, a convenient option for Typhoon Linda case study for simulation of wave parameter in nearshore areas. The coarse grid datasets of WW3 and WAM models ranged from 1°S to 24°N and from 90°E to 115°E in 51×51 equidistant grids with a resolution of 0.5° (Fig. 2). The model domain was finalized after checking the sensitivity connected to the SWAN model domain. The multi grid domains used in the SWAN model consisted of three domains ranging from 1.0°N to 23.0°N and 96.0°E to 118.0°E in d01, 3.0°N to 16.00°N and 98.0°E to 111.0°E in d02, and from 7.6°N to 13.6°N and 99.0°E to 105.0°E in d03. The nested grid resolutions of the coarse (d01), intermediate (d02) and fine (d03) domain equidistant grids were 926 m, 463 m and 46.3 m, respectively [8]. The nesting ratios of wind-wave model enables to simulate remotely generated swells in the SCS propagating into the GoT, and to reduce expensive high-resolution grids for the entire domain. Gridded bathymetry datasets are global data obtaining from the General Bathymetric Chart of the Oceans (GEBCO) with a 30 arc-second resolution and the STRM 15 plus with a 15 arc-second resolution [9]. Both gridded bathymetries with multi-survey datasets were employed in these domains. These gridded bathymetry datasets were generated by combining quality-controlled ship depth soundings with interpolation between sounding points guided by satellite-derived gravitational data. The digitized bathymetry data from multi-survey datasets of nautical charts of the Royal Thai Navy (bottom panel of Fig. 2) was merged to both gridded bathymetry datasets with a smooth sheet bathymetry by using the orthogonal grid maker. The SWAN structured grid model was constructed with the gridded bathymetry data that interpolated to each node to represent the bottom elevations of the wave model (Fig. 2). In this study, the WW3 model datasets were used as the IBCs for the coarse grid domain (d01) of SWAN model and the model results were re-compared with the wave pattern of the WW3 and WAM models.

The WW3 model including the *Hs*, mean wave direction and mean wave period was interpolated to points along the open boundary of the wave model to create parametric 'TPAR' files with a spatial resolution of 0.5°×0.5° and a temporal resolution of 3 h. These files were used by the SWAN wave model to compute JONSWAP spectra during the simulation. The wave frequencies were discretized from 0.04 to 1 Hz over 25 bins on a logarithmic scale and 36 bins with the resolution of 10° were taken for the direction. In this perspective, the utilization of

WW3 data was considered for a 10-year period (1999–2009) associated with the QSCAT satellite data and its computations for the investigation of the wind-wave resources and power assessments over the GoT and ADS.

E. Calculation method of Energy Density

Wind energy studies are commonly conducted at 10 m surface winds of offshore hybrid wind-wave energy converter system. The wind power density was calculated by 10 m wind speed. This quantity captures the flow of kinetic energy per unit area associated with the wind and is computed as

$$P_{wind} = 0.5\rho V^3 \quad (3)$$

where P_{wind} is the wind power density (W m^{-2}), V is the wind velocity (m s^{-1}), and ρ is the air density (1.292 kg m^{-3}).

The WW3 model datasets are the integral wind and wave parameters which can be used to calculate wind and wave power for every 3 h. The important integral wave parameters included the *Hs*, peak wave period (*Tp*), and mean wave direction (θ), which are derived from the simulated wave spectra. In deep water, the wave power per meter of wave crest can be obtained from the deep-water energy flux equation based on the *Hs* and mean wave period. It is evaluated as

$$P_{wave} = 0.42H_s^2T_p \text{ or } P_{wave} = 0.5H_s^2\bar{T} \quad (4)$$

where P_{wave} is the wave power density (kW m^{-1}), H_s is the significant wave height (m), T_p is the peak wave period (s), $\bar{T}$ is the mean wave period (s), and $T_p = 1.2\bar{T}$. Equations (3) and (4) above are the algorithms of wind and wave energy resources and power assessments by the Electric Power Research Institute (EPRI), USA.

In addition, the wind speed at 10 m above the sea surface of the QSCAT satellite and WW3 model datasets can be used for the alternative method to study the possibility of offshore wind energy resources and power assessments. The *Hf* calculated by the QSCAT satellite, and the *Hs* and $\bar{T}$ from the WW3 model datasets were also utilized with the same mission and objective as the wind power but it is for the wave power with a 10-year statistical analysis of offshore hybrid wind-wave energy assessments.

III. Results and Discussions

Generally, QSCAT provides continuous, accurate and high-resolution measurements of wind speeds and direction at 10 m above the ocean, regardless of weather conditions. It collects data covering 90% of Earth's surface each day. Bourassa *et al.* [10] had study on the wind retrievals with a spatial scale of 0.25° × 0.25° latitude/longitude and reported that the wind speed was measured in a range of 3–20 m s^{-1} with an accuracy of 2 m s^{-1} wind speed and 20° in direction. They also found that the root mean square differences between quality controlled research ships and QSCAT were approximately ±1 m s^{-1} in wind speed and ±15° in direction. The disadvantage of the QSCAT resolution was the spatial variability of wind field in coastal areas could not be captured. However, the QSCAT wind data can be downloaded for the swath mode format to the gridded mode which available twice per day. Due to the satellite sampling interval, the daily averages are not strictly comparable to numerical model output. Thus, the overview data used in this analysis, and the technical details of the analytical procedures are suggested to start with the QSCAT climatological and monthly mean datasets. These related issues may be useful to the use of other databases particularly for the three hourly analyzes of WW3 wind-wave power assessments over the same period of 1999–2009.

F. Overview of Climatological Data with Power Densities

The QSCAT average monthly wind speed was used to analyze the areas with possibility of high power in the GoT and ADS. In this study, the atmospheric circulation patterns with its dynamical processes presented in this section intend to illustrate the optimum ranges in wind-wave with its powers through the QSCAT data analysis. The QSCAT average monthly wind speed can be used to compute the wind power density (Eq.3), the *Hf* (Eq.1) and the simply wave period (Eq.2) by using the average water depth (Table 1) for the wave power density (Eq. 4). Fig. 1 presents that the QSCAT wind dataset covered the whole ADS, while it was limited to the GoT coast. Fig.3 also shows the areas of outstanding possibility of high wind and wave powers in the GoT and ADS. The temporal evolution of average monthly mean wind speeds (Fig. 3a) in the GoT and ADS was found that the monthly mean wind speeds were higher during the southwest monsoon (May to September) with a range of 4.8–8.0 m s^{-1} and relatively lower in summer (March to April) with a range of 4.2–5.3 m s^{-1}. The strongest mean wind speed was found in August, whereas the weakest one was in April.

In addition, the wind speed can be applied for the theoretical computations of the *Hf*, wind and wave powers (Eqs. 1–4) generated by the monsoonal winds and its circulations. During this monsoon season (rainy season in Thailand) over the GoT and ADS, the *Hf*, wind power and wave power were approximately 0.75–1.75 m, 100–300 W m^{-2} and 1.5–5.5 kW m^{-1}, respectively (Figs. 3b–3d). During the northeast monsoon (November to January), the climatological datasets with their analysis results provided more information and understanding of wind and wave circulation systems. Initially, the monthly mean of climatological data was analyzed for the offshore wind-wave energy resources and power assessments of both coasts (Fig. 3). The analysis results showed a clear annual cycle with the highest range over 6.0 m s^{-1} of wind speed, 1.0 m of H_f, 150 W m^{-2} of wind power and 1 kW s^{-1} in the ADS02 and GoT03 areas (red and purple color bars in Fig. 3b). Overall, it was clear that the annual cycle was dominated by low wave conditions during summer monsoon (in April) and high to highest wave conditions during transitional periods and winter monsoon.

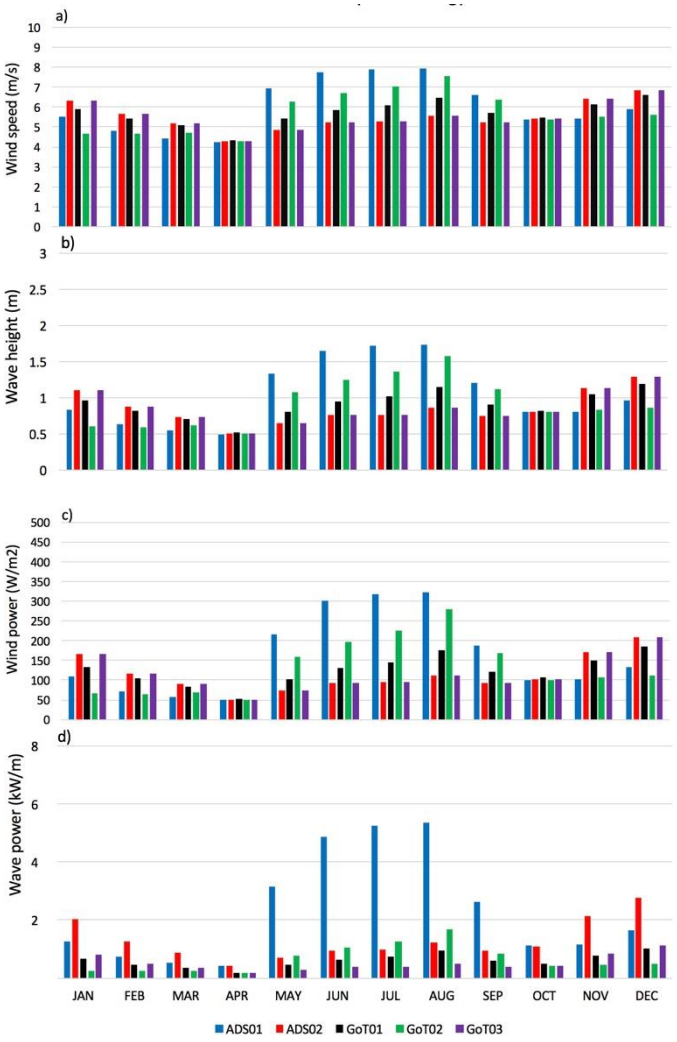

Fig. 3 Monthly a) wind speed (m s^{-1}), b) *Hf* (m), c) wind (W m^{-2}) and d) wave power (kW m^{-1}) densities over the GoT and ADS based on 10 years of QSCAT monthly climatology data and its computations at the areas of outstanding local possibility of high power.

G. Alternative Method of Monthly Power Densities

The quality of the calculation and simulation of wave height, wind and wave power densities depends mainly on the accuracy of the wind fields used. The wave heights approximately scale with the square of wind speed (Eq. 1). The driving wind fields with an error of about 10% resulted in an error of at least 20% in the hindcast wave height [11], while wind and wave power densities had more errors than 20% by the driving wind fields and hindcast wave height. In this study, the quality of the QSCAT wind fields were approximately analyzed for ±1 m s^{-1} in wind speed and ±15° in direction. It indicated that the QSCAT wind data was qualified for the computation and analysis of the *Hf*, wind and wave power densities for long-term hindcasts by using the offshore wind data analysis over 10-year period (1999-2009).

To consider dominant seasonal cycles and variations while focusing on long-term variation of the wind speed, simplified methods for estimating the *Hf* and its power densities, these average monthly wind speed and its computations were presented in time series (Fig. 4) over the subdomain of Fig. 1 as shown in Table 1. In this study, the seasonal cycles and their variations of each time series were a general inductive approach for qualitative data analysis of wind, wave and their power density variations of each time scale for several years. For the time series, the cycle of wind-induced waves and their power generation systems was approximately 10 cycles of the whole study period from 1999–2009 (Fig. 4). This feature is consistent with the QSCAT monthly climatology results from May to September, while longer time period provides more details of a weather pattern from a robustness of a small signal stability application of wind speed, wave height and their power densities. These are significantly higher than those monthly climatology results. In Fig. 4, the highest mean wind speed, wave height and their power densities were found during May to September, while the lowest values were presented during March to April. In the ADS01 and ADS02 regions, the mean wind, *Hf*, wind power and wave power during May to September were in the ranges of 8–9 m s^{-1}, 1.5–2.0 m, 200–450 W m^{-2} and 2.0–8.0 kW s^{-1}, respectively, while those presented during February to April were relatively lower with the ranges of 4–7 m s^{-1}, 0.5–1.5 m, 50–200 W m^{-2} and 0.5–2.0 kW s^{-1}, respectively, over both domains (Fig. 4).

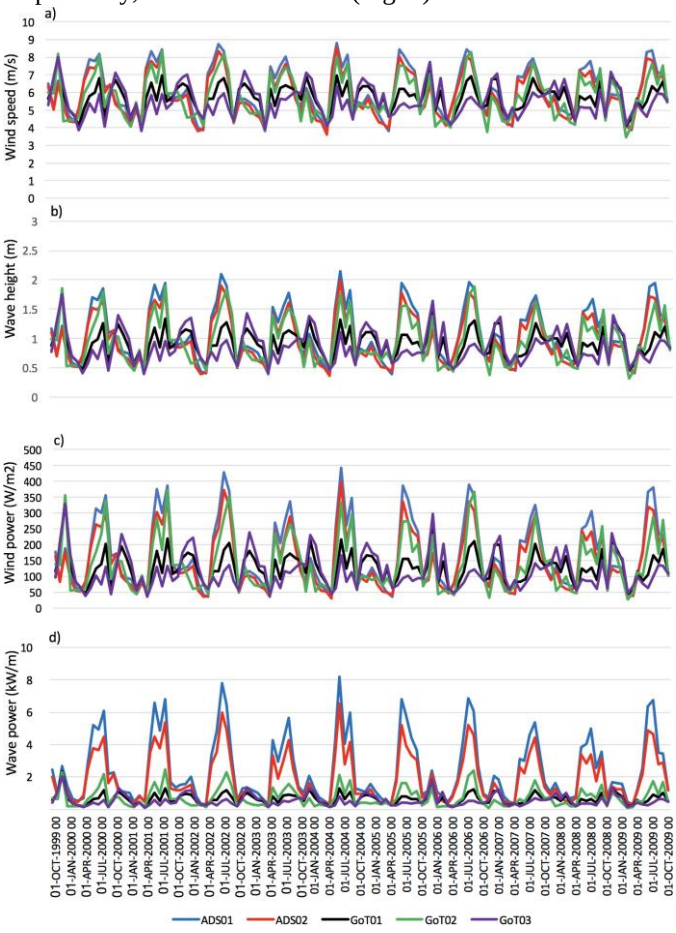

Fig. 4 Monthly a) wind speed (m s^{-1}), b) *Hf* (m), c) wind (W m^{-2}) and d) wave (kW m^{-1}) power densities over the GoT and ADS based on 10 years of QSCAT monthly mean data (1999-2009) and its computations at the areas of outstanding local possibility of high power.

In the upper GoT (GoT02), the H_f, wind speed, and their power densities during July to August were also up to 2 m, 8 m s^{-1}, 400 W m^{-2} and 2 kW s^{-1}, respectively. On the other hand, their lowest values were presented in the ranges of 0.5–1 m, 4–5 m s^{-1}, 50–150 W m^{-2} and 0.5–1.25 kW s^{-1}, respectively, during March and April. However, the GoT could be a potential area for wind and wave energy harvesting, particularly during the winter monsoon (November to January). The impact of strong winter monsoon plays an important role in the seasonal kinetic energy variability for the offshore wind and wave dynamical motions which could provide enough powers for the power generation device of a hybrid offshore renewable energy conversion system in the GoT. The greatest values of mean wind speed, *Hf* and their power densities during November and January were approximately 1.0–1.5 m, 6–8 m s^{-1}, 100–300 W m^{-2} and 1.5–2.0 kW s^{-1}. Their magnitudes and powers over the GoT area were higher than those of the ADS area during the same period of November to January.

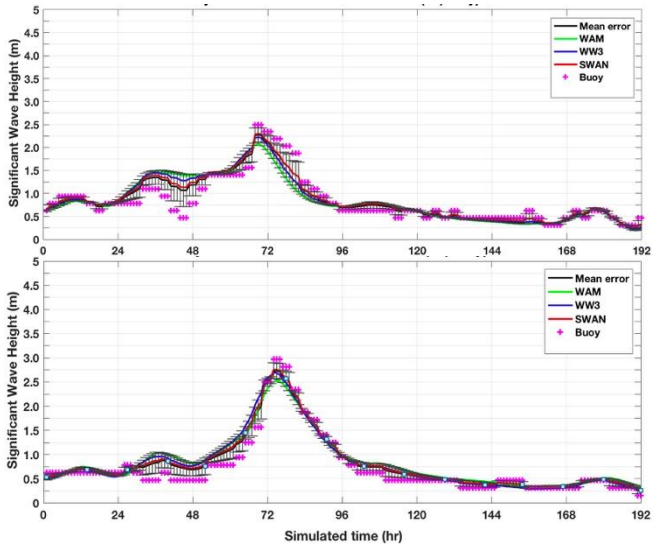

Fig. 5 Time series of SWAN-WRF model, WAM-ECMWF and WW3-NCEP datasets with error bar of standard deviation for H_s (m) at Ko Chang (102.21ºE,12ºN) and Rayong (101.23ºE,12.51ºN) buoys during the Typhoon Linda located in the GoT.

H. Alternative method of Three Hourly Energy Density

Much more focus has been given to the production of wind and wave energies. The most interesting fact is that the ocean can produce a huge amount of energy from wind and wave. An appropriate assessment of the *Hs* from the global WW3 data forced by the CFSR data can be the preliminary data for hybrid offshore wind-wave renewable energy conversion [12]. Extensive inter-comparison of H_s estimated from the WW3 and WAM reanalysis datasets (ECMWF-ERA-I, NCEP-CFSR against Ko Chang and Rayong buoys and the SWAN-WRF coupled model has been performed for the offshore consideration of Typhoon Linda 1997. Evaluation of the reanalysis datasets was based on the comparison between the available observation of the local buoys and the SWAN model results with high frequency and resolution of the *Hs*. This study showed that the SWAN model results with the open boundary conditions of the WW3 IBCs and the surface forced by the WRF model with ECMWF-ERAI IBCs could capture temporal variability with better performance (0.91 correlation coefficient) at the Ko Chang buoy with respect to other reanalysis data, i.e., the WW3-NCEP (0.84 in correlation coefficient) and the WAM-ECMWF (0.81 in correlation coefficient) datasets. The comparison of measured *Hs* data and reanalysis datasets of SWAN model simulation, WW3 and WAM presented high correlations (0.93 for SWAN, 0.90 for WW3 and 0.89 for WAM) with small root mean square errors (0.27 m for SWAN, 0.29 m for WW3, 0.32 m for WAM) at the Rayong buoy location (101.23ºE, 12.51ºN) during Typhoon Linda entering the GoT. The positive biases of WW3 and WAM model datasets were 0.10 m and 0.12 m, respectively, whereas the bias of SWAN model was slightly lower with a value of 0.09 m. However, these results presented that the *Hs* from the SWAN model simulation, WW3 and WAM model datasets were in good agreement with the observations (small differences) (Fig. 5). Thus, the WW3 datasets can be used for the alternative method for the long-term analysis trends with the seasonal and annual cycle considerations as well as the QSCAT data analysis for the wind-wave power assessments as shown in Figs. 6–7.

Performance of the WW3 model (global model datasets) forced by the NCEP-CFSR reanalysis data have been improved by comparing with satellite altimetry and buoy observations [13]. The WW3 model has been used to identify systematic seasonal biases, temporal and spatial error trends in terms of wind speed, wave height and swell. In this study, the time series plots of wind speed, *Hs* and mean wave period with their computations for wind and wave powers exposed the possibility of high power density of wind and wave energy sources as well as the interested areas of QSCAT data (Table 1). The WW3 model datasets showed the dominant features including large seasonal cycles through the wind and wave patterns for the power assessments from 1999–2009 as shown in Fig. 6. The WW3 model dataset had considerable influence on seasonal variations in wave and also provided similar features with the wind speed of QSCAT data (Figs. 4a vs. 6a). The higher frequency of WW3 model dataset for three hourly time intervals implies a smoother dataset providing detailed processes and weather extremes over the ADS.

The WW3 and QSCAT datasets showed the relationship of wind and wave datasets through the seasonal wind cycles over the ADS indicating a strong relationship between the CFSR data and satellite observation which explicitly accounted for an atmosphere stability. The WW3 model dataset forced by the CFSR data gave high predictions of wind in the ADS carrying to the wave predictions extending to the swell-dominated regions of ADS01 and ADS02. The WW3 wind speed showed similar trend with that of the QSCAT. It has a reasonably stable trend with the predictions getting more accurate in recent years. The trend lines demonstrated that the seasonal wind quantified for the independence of severity of wind and wave events implying consistent performance of WW3 and QSCAT datasets.

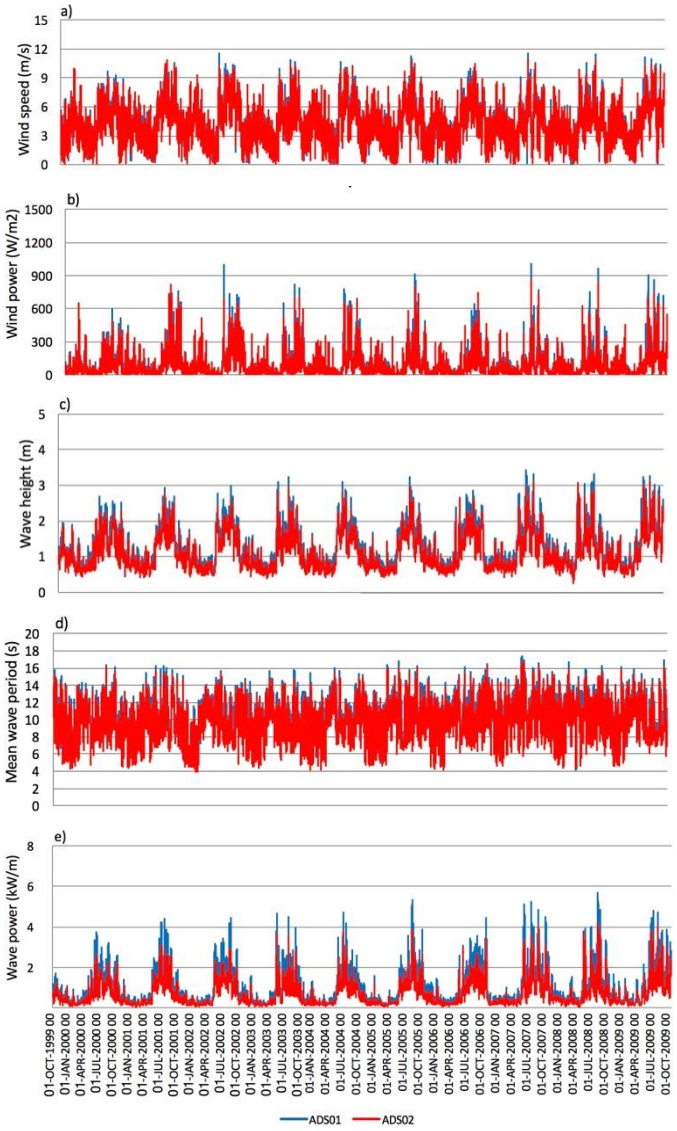

Fig. 6 Long-term data of WW3 datasets available (1999-2009) in three-hourly time intervals of a) wind speed (m s^{-1}), b) wind power density (W m^{-2}), c) *Hs* (m), d) mean wave period (s) and e) wave power (kW m^{-1}) in the ADS.

In this study, the three hourly intervals of wind speed, wind power, *Hs*, mean wave period and wave power during May to September (maximum) over the ADS01 and ADS02 were 9.0–11.8 m s^{-1}, 600–1000 W m^{-2}, 2.0–3.2 m, 14–17 s, and 2.0–5.9 kW s^{-1}, respectively. During February to April (minimum), those were reported in the ranges of 0.2–5 m s^{-1}, 10–550 W m^{-2}, 0.5–2.0 m, 4–12 s, 0.15–1.75 kW s^{-1}, respectively, over the subdomains of ADS (Fig. 6). In addition, the WW3 global model datasets presented an alternative method to analyze the wind-wave power densities in the shallow water of the GoT. It focused on the interplay of seasonal winds for offshore energy resources and power assessments over the GoT (Fig. 7). In winter season during November to January, the wind speed, wind power, *Hs*, mean wave period and wave power in the GoT03 were presented as 0.5–14 m s^{-1}, 50–1700 W m^{-2}, 0.5–3.2 m, 3.5–9.0 s, and 0.2–4.3 kW s^{-1}, respectively, while those found in the upper GoT (GoT02) during May to September (maximum) were 3.0–12.1 m s^{-1}, 50–1200 W m^{-2}, 0.4–2.3 m, 3–8.2 s, and 0.2–2.0 kW s^{-1}, respectively. Overall, the average wind speed and wind power were approximately 0.2–11.8 m s^{-1} and 50–900 W m^{-2}, respectively, whereas the *Hs*, mean wave period and wave power were found in the ranges of 0.2–2.9 m, 3.5–9 s, and 0.2–2.8 kW s^{-1}, respectively, over the GoT (GoT01) as shown in the black line of Fig. 7.

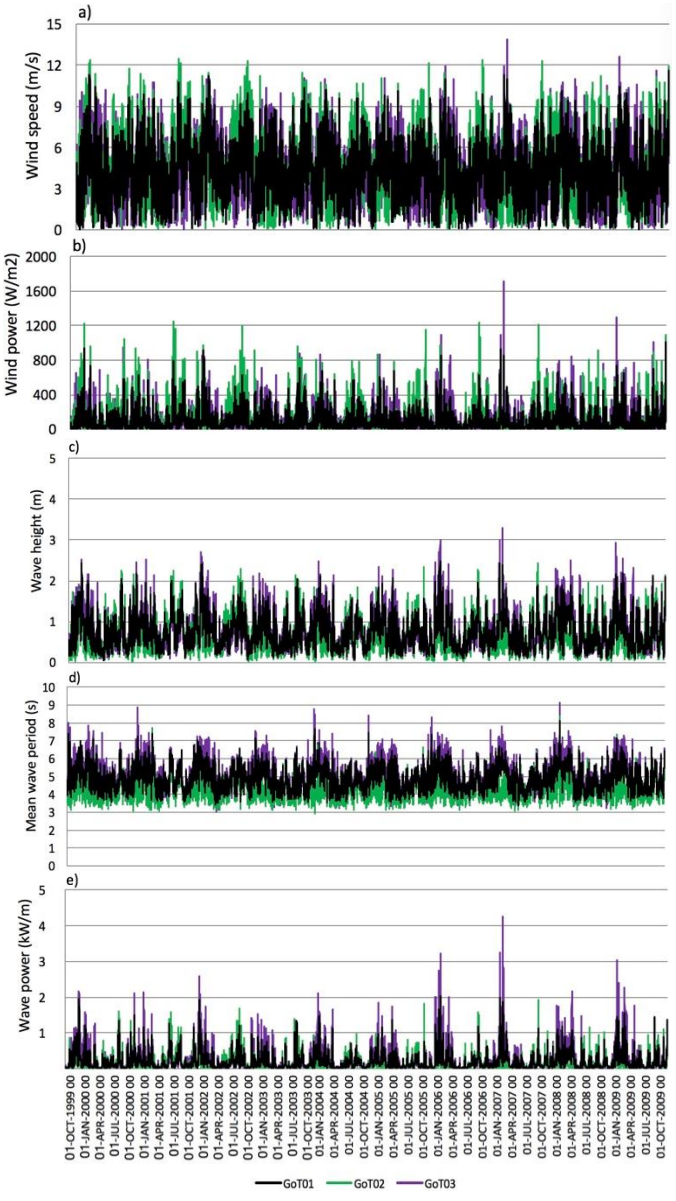

Fig. 7 Long-term data of WW3 datasets available (1999-2009) in three-hourly time intervals of a) wind speed (m s^{-1}), b) wind power density (W m^{-2}), c) *Hs* (m), d) mean wave period (s) and e) wave power (kW m^{-1}) in the GoT.

In summary, the WW3 was suitable for the studies of multi-years (1979–2009) with a high frequency of three-hourly interval for the seasonal cycle of wind-wave and its power density considerations and analysis. The QSCAT wind data provided additional capabilities for the analysis of extreme events but caution must be taken with the data discontinuity. For further study, the improved simulations and measurements

of wind and wave would provide further insights and explanations in high power density areas with the high resolutions of SWAN long-term simulations. The methodology and results presented in this paper would be a template and benchmark for evaluation of further analysis.

IV. Conclusions and Recommendations

The offshore wind-wave resources and power assessments of the GoT and ADS were investigated based on combinations of the QSCAT wind observation datasets from the JPL-NASA and the WW3 global model datasets from the NOAA/NCEP. Specifically, the WW3 datasets showed that GoT03 was the area of outstanding possibility of high power densities for a hybrid offshore renewable energy conversion, consisting of offshore wind and wave power generations. The results indicated that wind and wave capacities at the lower GoT covering the GoT03 could be generated in the ranges of 400-800 W m^{-2} and 1-1.5 kW m^{-1}, respectively. The GoT02 was also the suitable area for offshore wind power development with the wind capacity of 400-800 W m^{-2}. For the ADS01 whole domain and ADS02 inner domain, the WW3 model datasets and the monthly mean global climatology of QSCAT wind data presented wind and wave powers in the ranges of 300-600 W m^{-2} and 2-4 kW m^{-1}, respectively, harvesting from May to January. It showed the high quality of energy assessments for the wind-wave power production.

In addition, as previously mentioned (Fig. 5), the WAM reanalysis datasets with temporal resolution of 6 h by using the spatial resolution of 0.5º from the ECMWF-ERAI was applied to accurately force a wind-wave model. It could be a convenient approach to provide meteorological boundary condition and also could be compared with other models for the pattern analysis. In this study, a three-layer nested WRF model with 1 h temporal resolution and 1.33 km (d03) spatial resolution was implemented and used for driving the SWAN wind-wave model over the GoT for the climatological simulations and power assessments.

In the future study, the assessments of wind-wave energy and its power density in the SCS, GoT and ADS will be performed by using a fully coupled model, the Coupled Ocean Atmosphere Wave Sediment Transport (COAWST) modelling system with the consideration of wave-current interaction using the SWAN coupled with the Regional Ocean Modelling System (ROMS).

Acknowledgment

The authors would like to acknowledge the Asian Wave and Tidal Energy Conference (AWTEC) for its registration fee support. We are grateful to the National Science and Technology Development Agency (NSTDA) for its financial support of Woraluck Hongto under the Junior Science Talent Project (JSTP) Foundation. We also thank Dr. Sharon DeCarlo of the School of Ocean and Earth Science and Technology, University of Hawaii, for her technical support.

References

[1] H. L. Tolman, B. Balasubramaniyan, L. D. Burroughs, D. V. Chalikov, Y. Y. Chao, H. S. Chen, and V. M. Gerald, "Development and implementation of wind-generated ocean surface wave modelsat NCEP," *Amer. Meteor. Soc.*, vol. 17, pp. 311–333, Apr. 2002.

[2] N. Booij, R. C. Ris, and L. Holthuijsen, "A third-generation wave model for coastal regions, part II: verification," *J. Geophys. Res.*, vol. 104, pp. 7667–7681, Jan. 1999.

[3] J. C. Warner, B. Armstrong, R. He, and J. B. Zambon, "Development of a Coupled Ocean-Atmosphere-Wave-Sediment Transport (COAWST) modeling system," *Ocean Modeling*, vol. 35, pp. 230–244, 2010.

[4] W. Wannawong, D. Wang, Y. Zhang, and C. Ekkawatpanit, "Sensitivity of different parameterizations on simulation of tropical cyclone Durian over the South China Sea using Weather Research and Forecasting (WRF) model," *Preprints*, 2018040336, 2018.

[5] W. T. Liu and W. Tang, "Equivalent neutral wind," *JPL Publication*, 1996.

[6] K. A. Hilburn, F. J. Wentz, D. K. Smith, and P. Ashcroft, "Correcting active scatterometer data for the effects of rain using passive radiometer data," *J. Appl. Meteorol. Climatol.*, vol. 45, pp. 382–398, 2006.

[7] Coastal Engineering Research Center, Shore Protection Manual. U.S. Army Corps of Engineers, Waterways Experiment Station, Vicksburg Mississippi, 1984.

[8] S. Seemanth, B. Aich, K. Raj, and S. Rashmi, "Sensitivity analysis of dissipation parameterizations in a third-generation spectral wave model, WAVEWATCH III for Indian Ocean," *Ocean Eng.*, vol. 124, pp. 252–273, 2016.

[9] J. O. Christopher, J. B. Joseph, and T. S. David, "Data fusion of Shuttle Radar Topography Mission (SRTM) land topography with measured and estimated seafloor topography," NCEI Accession 0150537, Version 1.1. NOAA National Centers for Environmental Information. Dataset, 2016.

[10] M. A. Bourassa, D. M. Legler, J. J. O'Brien, and S. R. Smith, "SeaWinds validation with research vessels," *J. Geophys. Res.*, vol. 108, Feb. 2003.

[11] H. L. Tolman, "Validation of NCEP's ocean winds for the use in wind wave models," *Global Atmos Ocean Sys*, vol. 6, pp. 243–268, 1998.

[12] S. Caires, A. Sterl, J. R. Bidlot, N. Graham, and V. Swail, "Intercomparison of different wind–wave reanalysis," *J. Clim.*, vol. 17, pp. 1893–1913, 2004

[13] J. E. Stopa and K. F. Cheung, "Intercomparison of wind and wave data from the ECMWF Reanalysis Interim and the NCEP Climate Forecast System Reanalysis," *Ocean Modelling*, vol. 75, pp. 65–83, 2014.